EFFICIENT SIMULATION OF INLET DISTORTION IN ENGINE FAN STAGE USING NONLINEAR HARMONIC METHOD

Omid Z. Mehdizadeh, Stéphane Vilmin, Benoît Tartinville, Charles Hirsch

NUMECA International, Brussels, Belgium
omid.mehdizadeh@numeca.be, stephane.vilmin@numeca.be,
benoit.tartinville@numeca.be, charles.hirsch@numeca.be

ABSTRACT

The nonlinear harmonic method (NLH) for efficiently simulating unsteady turbomachinery fluid dynamics in the frequency domain is described, and the details of its application to inlet distortion are discussed. The method capabilities are then demonstrated on the NASA transonic fan Stage 67 with a generic inlet distortion. Comparison of the results with the available experimental data confirms that the reconstructed unsteady flow solution obtained by the nonlinear harmonic method captures the main flow characteristics of the inlet distortion interaction with the fan stage such as the swirl associated with the upstream flow redistribution, the total pressure distortion transfer, and the generation of the total temperature distortion.

The method offers a cost saving of two orders of magnitude compared to conventional time-domain unsteady methods for this type of applications.

KEYWORDS

Harmonic, distortion, fan, transonic

NOMENCLATURE

P	pressure
t	total (stagnation) quantity, subscript
T	temperature
$y+$	non-dimensional wall distance
0	reference value, subscript

Acronyms

CFD	computational fluid dynamics
LE	leading edge
NLH	nonlinear harmonic method
TE	trailing edge

INTRODUCTION

Inlet flow distortion can undermine the performance, stability, and durability of gas turbine engines, due to the unsteady interaction with the fan stage or the first compressor stage (Longley and Greitzer, 1992). This unsteady interaction can deteriorate the flow conditions in the flow passages that rotate through the distorted region. Different levels of inlet distortion may occur during the operation of aircraft engines. It can be constantly present due to propulsion-airframe integration, or it can occasionally happen due to aircraft maneuvers or crosswind. Therefore, it should be of importance to better understand the propagation of distortion into the fan or the first

compressor stage and to be able to integrate such an analysis into the design cycle (Cousins *et al.*, 2017).

However, the accurate simulation of inlet distortion effects using conventional unsteady CFD methods requires large computational resources since the complete wheel must be included (*i.e.*, all the flow passages), and the unsteady computation must typically run for several revolutions in order to converge to a periodic state (Yao *et al.*, 2008, Jerez Fidalgo *et al.*, 2012, Zhang and Vahdati, 2017, Bakhle *et al.*, 2018). Solving such a problem into the frequency domain – instead of the time domain – is computationally more efficient. Indeed, using such a method allows to take full advantage of the periodic nature of the configuration – both in time and in space. The nonlinear harmonic method (NLH) has already demonstrated its capabilities of accurately and efficiently treating turbomachinery configurations that are subject to perturbations coming from blade passing as well as blade vibrations (Vilmin *et al.*, 2013, Debrabandere *et al.*, 2015). It is here proposed to apply this method to perturbations generated by inlet distortion.

In the following sections, first the NLH method is introduced and its application to inlet distortion is further discussed. Then, its effectiveness for the analysis of inlet distortion is demonstrated on the NASA transonic fan Stage 67.

METHODOLOGY

Flow Solver

The solver used in this work is part of the FINE^{TM}/Turbo package, which is a complete CFD software suite from grid generation to flow visualization dedicated to turbomachinery applications. The flow solver is a density-based Navier-Stokes code using a block-structured, finite-volume method. The spatial discretization is a second order central difference scheme with a Jameson type artificial dissipation, and the pseudo-time marching method uses a four-stage explicit Runge-Kutta scheme. The turbulence model of Spalart and Allmaras (1992) is used in the present study. Convergence acceleration techniques such as multi-grid, local time-stepping, and implicit residual smoothing are used in order to reduce the computation time. All the details of the flow solver can be found in the software documentation (NUMECA, 2018).

Nonlinear Harmonic Method

The flow solver features a highly efficient frequency-domain method for the computation of periodic unsteady flows in turbomachinery applications called the NLH method. The method, which was originally published by He and Ning (1998), has been further developed and implemented in the solver by Vilmin *et al.* (2006, 2013). Since its introduction in the solver, the method's capabilities have been continuously extended, covering an ever-wider range of applications, including the extension to fluid-structure interaction (Debrabandere *et al.*, 2015) and conjugate heat transfer (Mehdizadeh *et al.*, 2017).

The method is based on splitting each unsteady conservative flow variable into a time-mean part and a time-fluctuating part that is assumed to be the sum of periodic perturbations with given frequencies (such as the blade-passing frequencies). Each periodic perturbation is then Fourier-decomposed into a user-specified number of harmonics, each of them defined by a real and an imaginary part (retaining both the amplitude and the phase information). In other words, the set of the five unsteady conservative flow variables are transformed from the time domain to the frequency domain resulting in a set of five time-mean variables and additional sets of ten harmonic variables for each of the user-specified number of harmonics. For instance, for a blade row in between two other rows, when the number of harmonics for each perturbation is set to three, there will be a total of six sets of ten harmonic variables in addition to the set of five time-mean variables.

The transport equations for the set of the time-mean variables are obtained by time-averaging the unsteady Navier-Stokes equations, and as a result include the so-called deterministic stress terms, formally similar to Reynolds stresses in turbulence. These stress terms are the time-mean values of the products of the harmonic fluctuations due to the nonlinear terms of the Navier-Stokes

equations such as the kinetic term of the momentum equation. The inclusion of the stress terms enhances the accuracy of the time-mean solution compared to the conventional steady-state solution. This is why the method is said to be nonlinear as opposed to a linear frequency domain method.

Each set of the harmonic variables is solved with a set of transport equations that is obtained by casting the first-order linearized Navier-Stokes equations into the frequency domain. Thanks to the azimuthal periodicity of the row, each harmonic variable, like the time-mean variables, can be solved in a single interblade channel. In the frequency domain, its values at the azimuthal periodic boundaries are connected by the interblade phase angle, which is the ratio between the azimuthal periodicity of its generator and that of the row (He and Ning, 1998). Thus, the size of the computational domain is kept to a minimum. A 1D local non-reflecting treatment based on the characteristics is applied for the primitive harmonic variables at the inlet and the outlet boundaries. The harmonic equations, along with the time-mean equations, are solved by the same explicit pseudo-time marching scheme, which performs the convergence to a pseudo-steady state in the frequency domain.

The converged solution, obtained in a single passage, is then used to reconstruct the full unsteady flow (*i.e.*, the time-mean plus the perturbations) all over the full wheel using the interblade phase angle information. Hence, the overall computational cost is remarkably affordable, and it is much smaller than the conventional time-marching methods for unsteady flow solution, which often require the computation of numerous time steps on the full wheel.

Inlet Distortion Boundary Condition

When the flow at the rotor inlet boundary is non-uniform in the circumferential direction, each rotor blade is subject to a periodic flow perturbation with a given frequency, which depends on the rotational speed of the rotor and the number of repetitions of the inlet distortion profile. Therefore, rotor inlet distortion can as well be efficiently simulated with the NLH method. This is also similarly applicable to the stator inlet boundary by means of space harmonics instead of time harmonics (see for example Mehdizadeh *et al.*, 2017).

The primitive harmonic variables at the inlet are determined in two steps, one during the preprocessing and the other during the iterations. First, the harmonics of the specified quantities at the inlet (*e.g.*, total pressure and total temperature) are obtained by means of Fourier decomposition along the circumferential direction (and relative rotation in the rotor frame). Second, at each iteration, the primitive harmonic variables are obtained from the given quantities using first-order linearized thermodynamic relations. Note that the mean variables at the inlet are determined in the same manner as for a uniform flow by means of averaging the specified quantities at the inlet along the circumferential direction.

APPLICATION TO A FAN STAGE

To demonstrate the capabilities of the NLH method in simulating inlet distortion, the method is applied to the NASA transonic fan Stage 67. This test case has been the subject of a few publications where good agreements between the conventional time-domain unsteady solution and the experimental results have been reported (Jerez Fidalgo *et al.*, 2012 and Zhang and Vahdati, 2017). To the author's knowledge, the details of the experiment on the fan Stage 67 have not been published elsewhere than partly in these two papers. All the available data have been exploited but the results of the current study can be affected by a series of uncertainties. This is the case for the exact geometry of the test rig, the precise operating condition, the exact location of the measurement planes, and the error margin of the experimental data. However, even if a rigorous quantitative validation of the NLH method cannot be done with available data on this particular configuration, the capabilities of the method to reproduce the observed downstream propagation of the disturbance will be obvious.

Computational Domain

As illustrated in Fig. 1, the computational domain consists of only one blade passage per row, and it includes the spinner. The distance between the inlet and the rotor leading edge is six times the rotor axial chord at mid span, and the distance between the outlet and the stator trailing edge is three times the stator axial chord at mid span. Three axial stations of interest are also marked on Fig 1: St. 1 is at 2.5 times the rotor axial chord upstream of the rotor leading edge, St. 2 is at the rotor-stator interface, and St. 3 is at one stator axial chord downstream of the stator trailing edge. The rotor tip clearance is 0.51 mm.

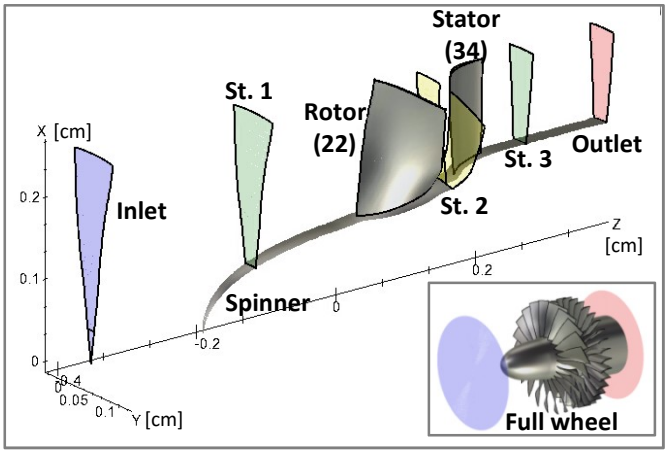

Figure 1: Computational domain (shroud and periodic boundaries not shown)

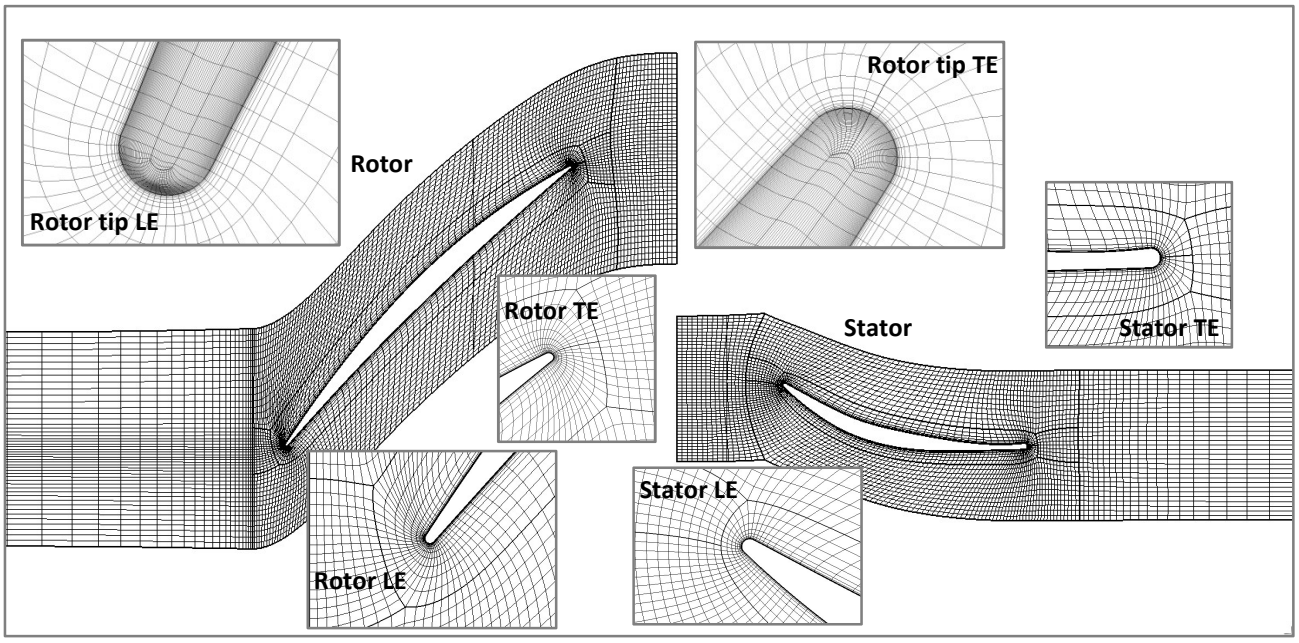

Figure 2: Blade-to-blade mesh at mid span (coarse grid level shown)

The block-structured mesh in the computational domain is generated by AutoGrid5^{TM}, which is part of the FINE ^{TM} /Turbo package. The mesh counts are 5.66 and 2.05 million points in the rotor and the stator domains, respectively. The number of points in the spanwise direction is respectively 113 and 81 (including the 33 points in the rotor tip clearance). The number of points in the tangential direction at the rotor-stator interface is 97 on both sides. The first cell height on all the solid walls is 1 μm leading to a y+ of the order unity. The mesh is considered sufficiently fine for this type of application according to our experience and the industry common practice. This is confirmed in the Simulation Results section below, where the comparison of the results obtained on the fine and the coarse grid level (with half the number of points in each direction) shows low

sensitivity to the mesh. The mid-span blade-to-blade mesh is shown in Fig. 2, where only every second point is shown for clearer visualization (coarse grid level).

The rotational speed is set to 90% of the design speed (-14438.5 RPM). Air is modeled as a thermally perfect gas.

Boundary Conditions

At the inlet, total pressure, total temperature, and flow angles are imposed. Total pressure is imposed as an r-θ profile defined over the whole disk. As shown in Fig. 3 (black solid line), the profile in the circumferential direction is a rectangular function with the high value of 101.325 kPa and with a 10.5% drop in a 120-degree sector from 120 to 240 degrees. In the radial direction, the profile is mostly constant except within 1 mm of the casing wall where it linearly decreases from the local total pressure value to the expected static pressure value on the wall. Both total temperature and flow direction are uniform at the inlet, 288.15 K and axial respectively.

As described in the Methodology section above, the non-uniform total pressure profile is decomposed into a user-specified number of harmonics. This is illustrated in Fig. 3, where the reconstruction of the inlet total pressure profile over the whole circumference is shown with increasing number of harmonics from one to nine. Generally, as the number of harmonics increases, so does the accuracy of the profile representation. However, for this particular case where the extent of the lower pressure sector corresponds exactly to one third of the full circle, the amplitude of the harmonics three, six, nine (and all other multiples of three) should be zero. In the present investigation, maximum four harmonics are retained (up to the fifth harmonic, skipping the third harmonic) to represent the inlet total pressure profile in the Simulation Results section below. Since the "rank 2" harmonic method is selected, those four harmonics are present in both the rotor and the stator rows. In addition to the four inlet distortion harmonics, three harmonics are retained to represent the perturbation associated with the blade passing frequency of the adjacent row. So, overall, for the whole computational domain, seven sets of harmonic variables are solved in addition to the mean variables. It should also be mentioned that such a rectangular-shaped inlet distortion is more challenging for the NLH method than more classical distortions that are closer to pure sinus waves as for instance in Yao *et al.* (2008).

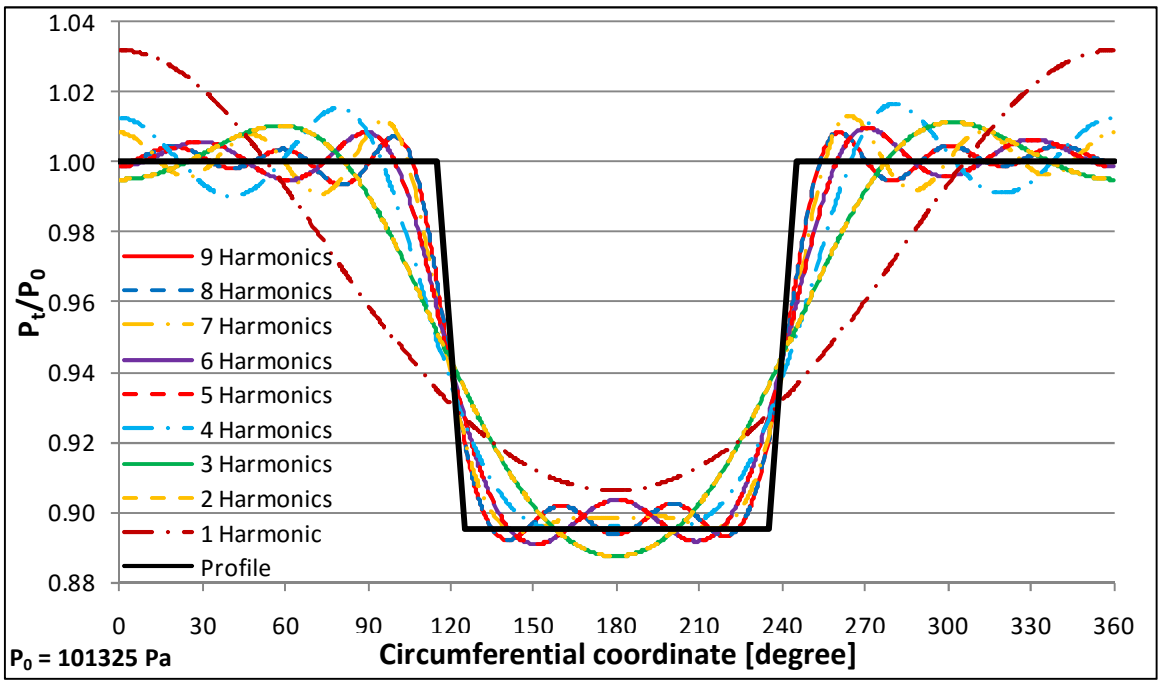

Figure 3: Inlet total pressure profile and its reconstructed harmonic representations

At the outlet, the solver automatically updates the radial equilibrium static pressure to achieve the desired mass flow rate. The outlet mass flow rate is set to 30.8 kg/s, which results in a rotor pressure ratio that matches the value reported by Jerez Fidalgo *et al.* (2012), in order to have a comparable operating point.

Simulation Results

The main performance parameters resulted from the simulation are listed in Tab. 1, where not only the rotor pressure ratio but also the rotor efficiency nearly matches those reported by Jerez Fidalgo *et al.* (2012).

Table 1: Resulting performance parameters

	Pressure ratio	Efficiency [%]
Rotor alone	1.46	92.4
Stage	1.43	87.4

As an overview of the flow solution, the reconstructed normalized instantaneous total pressure and total temperature contours at mid span are presented in Fig. 4 and Fig. 5, respectively. Total pressure distortion transfer and total temperature distortion generation through the fan stage is evident in these figures. Note that the low-pressure sector of the inlet total pressure profile is marked with two black dashed lines, A and B.

First of all, the inlet total pressure profile remains intact as it is convected from the inlet to the fan face. This indicates that the mesh size in the inlet duct is sufficiently fine relative to the wavelength of the inlet distortion harmonics to avoid any significant numerical dissipation of these harmonics. As the low-pressure flow is transferred through the rotor, it appears to slightly shift in the opposite direction of the rotor rotation (to the right). This is due to the presence of opposite local tangential flows near the boundaries of the low-pressure sector (marked with two white arrows), which are induced by the lower fan-face static pressure in the low-pressure sector. Near dashed line A, the local tangential flow is in the opposite direction of the rotor rotation resulting in a higher incidence angle and consequently higher total pressure ratio through the rotor. The opposite happens near dashed line B resulting in a lower total pressure ratio through the rotor.

The total temperature distortion is primarily due to the lower axial velocity in the low-pressure sector resulting in more turning (*i.e.*, more work input) by the rotor and consequently higher total temperature ratio. Furthermore, the local tangential flows again shift the generated distortion but in the opposite direction of that of the total pressure profile (to the left). This shift to the left is more pronounced since the distortion is further convected to the left by the turning flow in the inter-row space.

The opposite local tangential flows upstream of the rotor are evident in the flow angle plot shown in Fig. 6, where the flow directions point toward the center of the low-pressure sector with the maximum flow angle magnitudes near its boundaries (black dashed lines A and B). The plotted flow angles are extracted at mid span and at 2.5 times the rotor axial chord upstream of the rotor leading edge (St. 1). The red solid curve shows the NLH results with four harmonics representing the inlet total pressure profile plus three harmonics representing the rotor-stator interaction. It can be seen that the NLH results match the experimental data (black circles) fairly well, capturing both the trend and the level of the flow angle variations in the circumferential direction. Compared to the unsteady results of Jerez Fidalgo *et al.*, 2012 (black solid curve), the NLH results are smoother, which is a characteristic of a reconstructed harmonic solution with only a few harmonics. The impact of the number of harmonics on the solution can be seen by comparing the red solid curve with the blue dashed curve, which is obtained with half the number of harmonics representing the inlet distortion. Since the flow angle profile upstream of the rotor is rather simple, the two curves are similar as expected. For the same reason, the impact of the mesh is also expected to be small at

this station. Indeed, the red solid curve nearly covers the dotted green curve, which shows the results obtained on the coarse grid level with half the number of points in each direction.

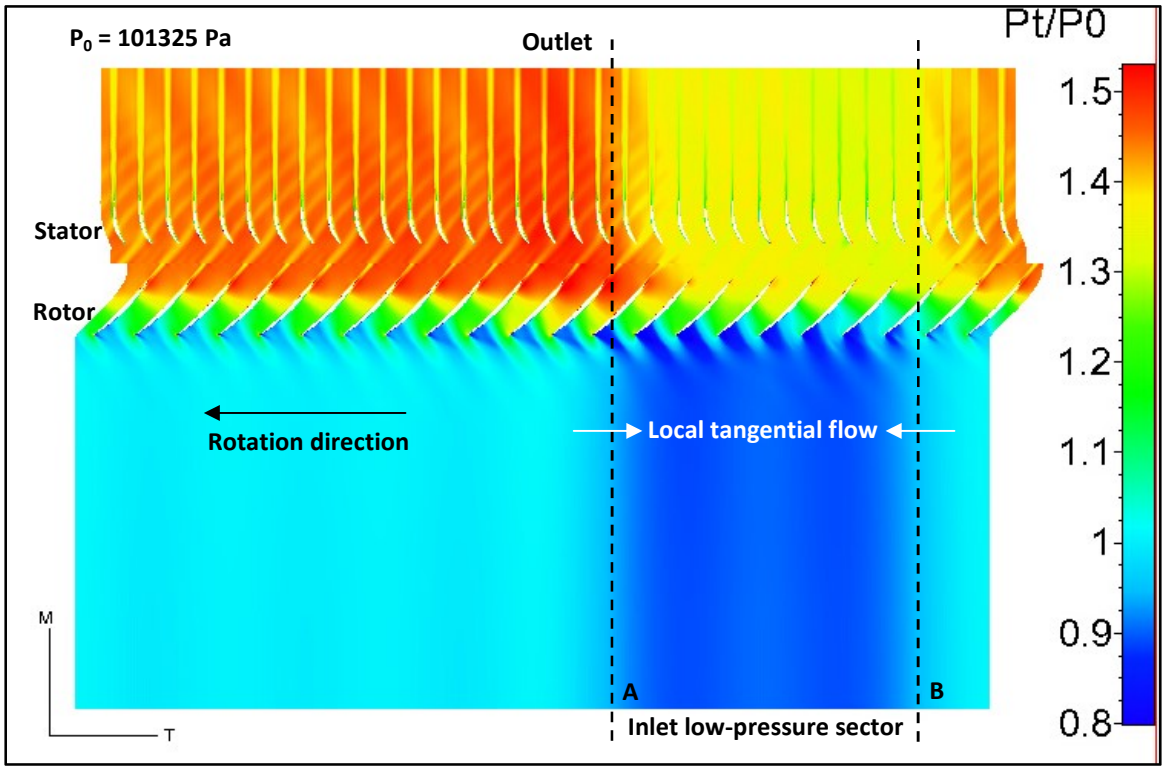

Figure 4: Mid-span blade-to-blade view of instantaneous total pressure contours

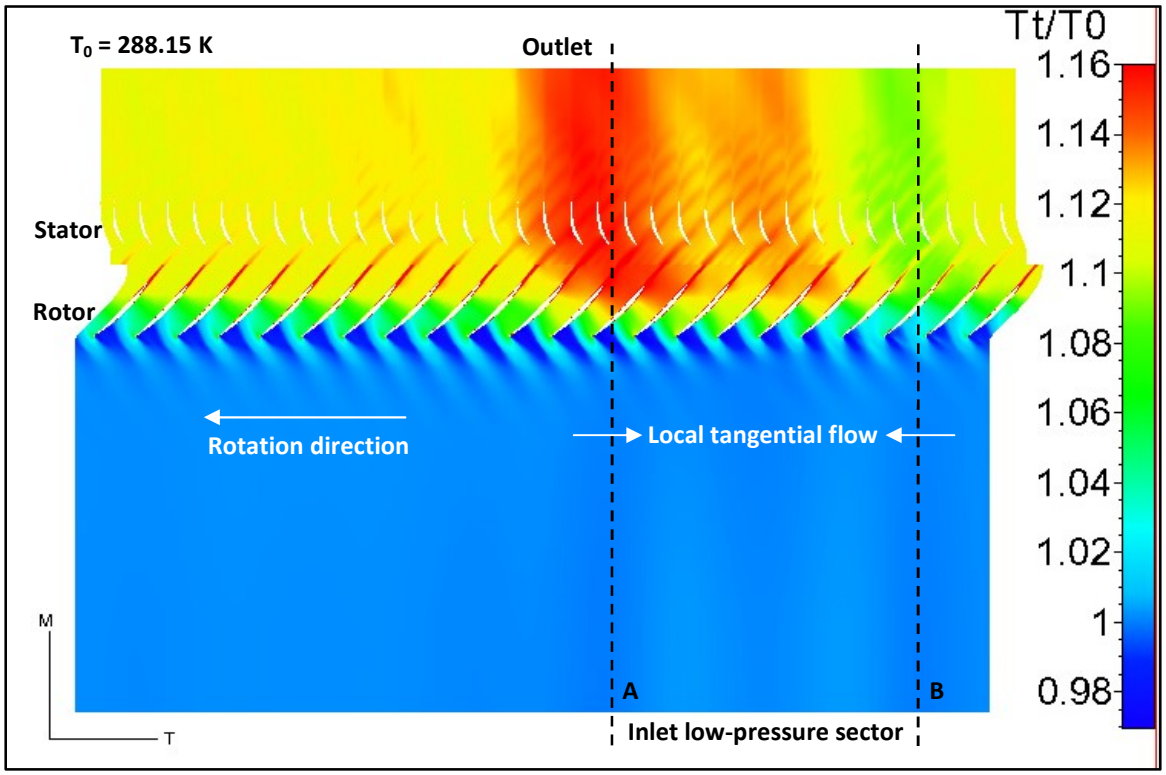

Figure 5: Mid-span blade-to-blade view of instantaneous total temperature contours

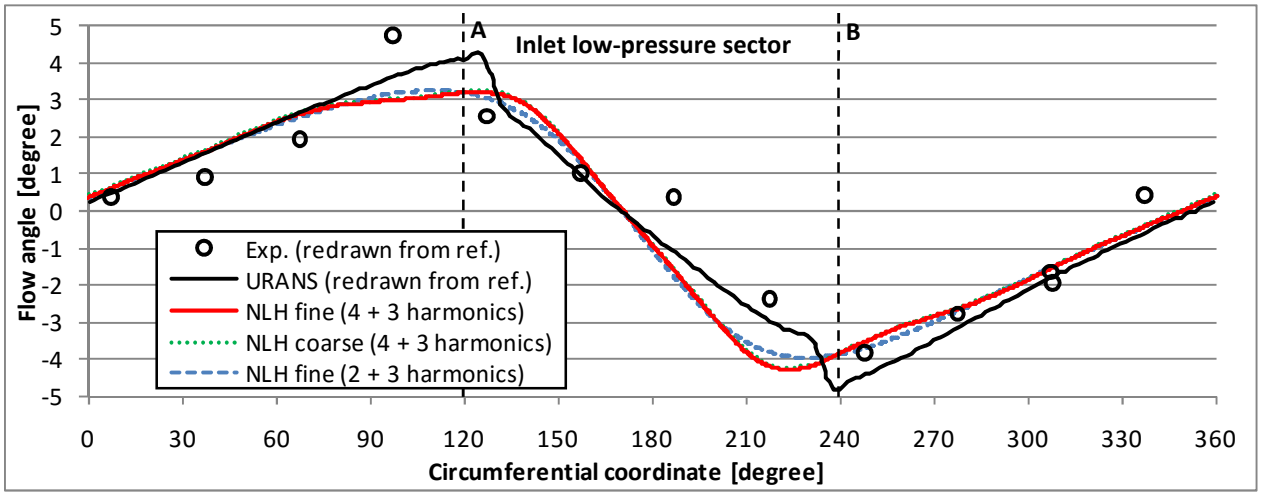

Figure 6: Mid-span flow angle distribution at St. 1 (upstream of the rotor), ref.: Jerez Fidalgo *et al.*, 2012

The total pressure and total temperature distributions downstream of the rotor (St. 2) are shown in Fig. 7(a) and 7(b), respectively. As expected, both distributions are quite different than those upstream of the rotor. As pointed out before, the low-pressure flow is shifted to the right (around 15 degrees) while the newly generated high-temperature flow is shifted to the left (around 20 degrees). Again, the NLH results (red sold curve) match the experimental data (black circles) fairly well in capturing the location and the level of the low-pressure and the high-temperature flows. Furthermore, their agreement with the experimental results is comparable with that of the unsteady results of Jerez Fidalgo *et al.*, 2012 (black solid curve). Note that the impact of the number of harmonics on the solution is quite evident here. While the solution with only two harmonics (blue dashed curve) does capture the main trend in a relatively smooth curve, the solution with four harmonics (red solid curve) captures more complexities, and it is more like the unsteady results of Jerez Fidalgo *et al.*, 2012 (black solid curve). Also, the impact of the mesh is more visible at St. 2 than upstream of the rotor, particularly in the total pressure plots, where the solution with coarser grid level (dotted green curve) shows slightly lower values. The small difference can be attributed to the slightly higher numerical dissipation on the coarser grid, and it confirms the low mesh sensitivity.

Fig. 7(c) and 7(d) show that the total pressure and total temperature distributions do not change much through the stator (at St. 3) except for a small shift to the left (around 10 degrees), which can be explained by the turning flow in the space between the rotor and the stator as mentioned before. The NLH results (red solid curve) again match the experimental data (black circles) fairly well and are comparable to the unsteady results of Jerez Fidalgo *et al.*, 2012 (black solid curve). Also, the same observations as above can be made regarding the impact of the number of harmonics as well as the impact of the mesh; the lower number of harmonics (dashed blue curve) leads to a relatively simpler curve, and the coarser grid level (dotted green curve) leads to a slightly lower total pressure due to slightly higher numerical dissipation.

Fig. 8 shows how the inlet distortion affects the flow structure downstream of the stator (St. 3) in both spanwise and circumferential directions. The stator corner separation near the shroud, identified by low total pressure (blue regions), is strongly affected by the inlet distortion, while a high total pressure jet is formed near the hub on the opposite side. Also, the clockwise shift of the low pressure flow is slightly smaller near the hub than near the shroud.

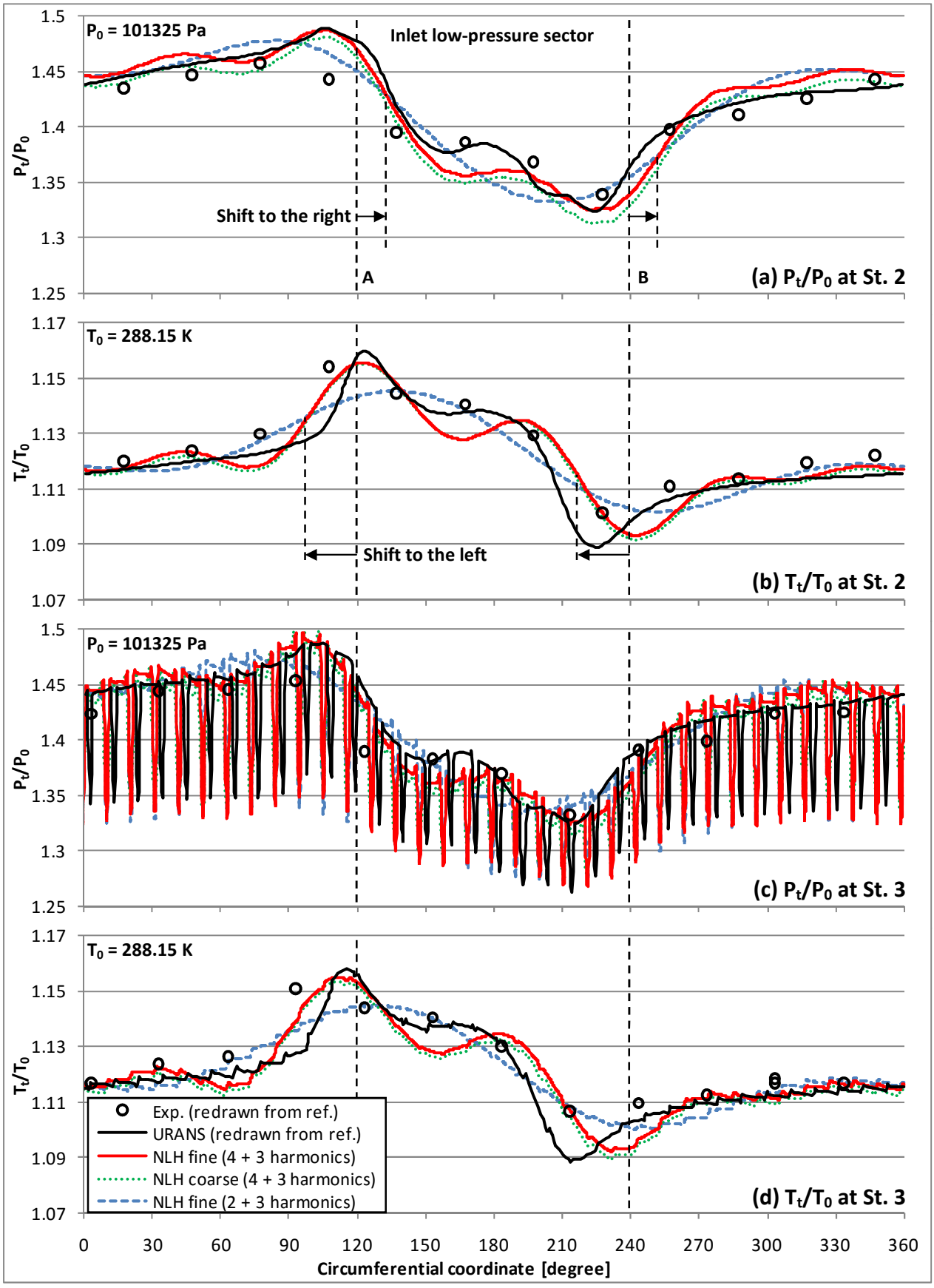

Figure 7: Mid-span time-mean total pressure and total temperature distribution at St. 2 (rotor-stator interface) and St. 3 (downstream of the stator), ref.: Jerez Fidalgo *et al.*, 2012

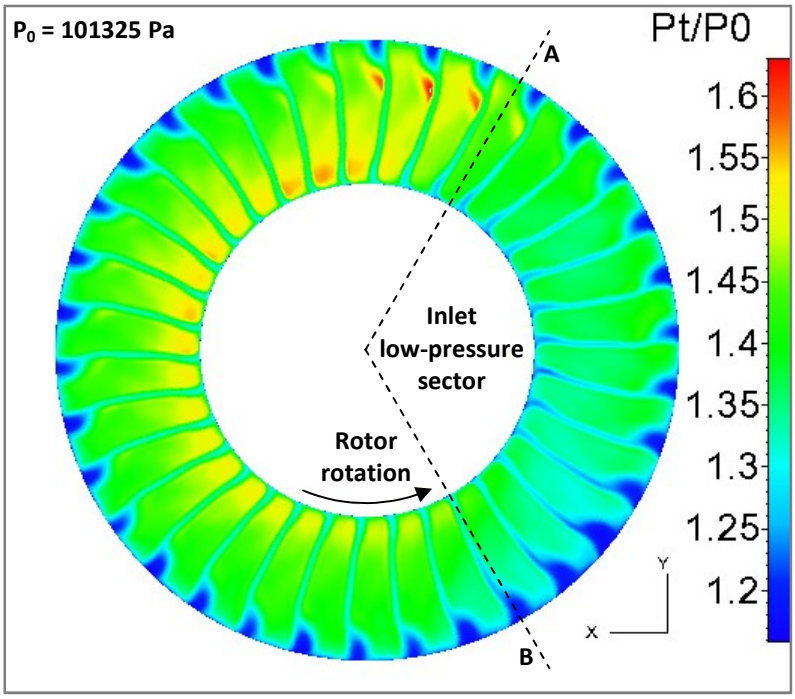

Figure 8: Axial view of instantaneous total pressure contours at St. 3

Computational Efficiency

The computation with 7 harmonics (four representing the inlet distortion plus three representing the rotor-stator interaction) takes around one day and a half on 16 processor cores to converge which is around 150 to 300 times faster than the reported times needed for the conventional time-domain unsteady computations of the same fan stage to converge (Jerez Fidalgo *et al.*, 2012). This confirms figures that have already been reported by Vilmin *et al.* (2013). In other words, the NLH method offers a cost saving of at least two orders of magnitude compared to the conventional unsteady methods for this type of applications. Note that the computations are considered converged when the trends of global parameters such as the inlet and outlet mass flow rates, the stage total pressure ratio, and the stage efficiency have stabilized and do not change with iterations anymore.

CONCLUSIONS

The nonlinear harmonic method of FINE^{TM}/Turbo has been applied to the NASA transonic fan Stage 67 facing a rectangular generic inlet distortion. Although such an inlet perturbation is challenging for a frequency domain method, the flow solver allows to accurately represent the propagation of the distortion into this fan stage and in particular downstream of the stator blades. This demonstrates the applicability of the NLH method to such a complex configuration at a drastically lower computational cost than a standard time-domain approach. Therefore, this methodology can be used to investigate the impact of inlet distortion on the performance, and potentially the stall margin, early in the design process.

Furthermore, as inlet distortion could also impact the structural integrity of the fan stage, the analysis could be extended to fluid-structure interactions using the NLH method coupled to a modal structural approach (González Horcas *et al.*, 2017) at an even more reduced cost than state of the art methods.

REFERENCES

Bakhle, M.A., Reddy, T.S.R., Coroneos, R., Min, J.B., Provenza, A.J., Duffy, K.P., Stefko, G.L., Heinlein, G. (2018). *Aeromechanics Analysis of a Distortion-Tolerant Fan with Boundary Layer Ingestion*. AIAA 2018-1891.

Cousins, W.T., Voytovych, D., Tillman, G. (2017). *Design of a Distortion-Tolerant Fan for a Boundary-Layer Ingesting Embedded Engine Application*. AIAA paper 2017-5042.

Debrabandere, F., Vilmin, S., Tartinville, B., Hirsch, Ch., Coussement G. (2015). *Application of the Non-Linear Harmonic Method to Flutter Calculation in Multi-Row Turbomachinery*. ETC2015-139

González Horcas, S., Debrabandere, F., Tartinville, B., Hirsch, Ch., Coussement G. (2017). *Extension of the Non-Linear Harmonic method for the study of the dynamic aeroelasticity of horizontal axis wind turbines*. J. Fluids & Structures, 73, pp 100-124.

He, L., Ning, W. (1998). *Efficient Approach for Analysis of Unsteady Viscous Flows in Turbomachines*. AIAA Journal, Vol. 36, No. 11.

Jerez Fidalgo, V., Hall, C.A., Colin, Y., (2012). *A Study of Fan-Distortion Interaction within the NASA Rotor 67 Transonic Stage*. ASME J. Turbomachinery, 134, 051011.

Longley, J.P., Greitzer, E.M. (1992). *Inlet Distortion Effects in Aircraft Propulsion system Integration*. AGARD Lecture Series 183, pp 6-1–6-18.

Mehdizadeh, O., Vilmin, S., Tartinville, B., Hirsch, Ch. (2017). *Nonleanear Harmonic Method Applied to Turbine Conjugate Heat Transfer Analysis for Efficient Simulation of Hot Streak Clocking and Unsteady Heat Transfer*. ASME Paper GT2017-63622.

NUMECA International (2018), *FINE^{TM}/Turbo User Guide 13.1.* www.numeca.be

Spalart, P.R., Allmaras, S.R. (1992). *A One-Equation Turbulence Model for Aerodynamic Flows.* AIAA paper 92-0439.

Vilmin, S., Lorrain, E., Hirsch, Ch., Swoboda, M. (2006). *Unsteady Flow Modeling Across the Rotor/Stator Interface Using the Nonlinear Harmonic Method*. ASME Paper GT2006-90210.

Vilmin, S., Lorrain, E., Tartinville, B., Capron, A., Hirsch, Ch. (2013). *The Nonlinear Harmonic Method: From single stage to multi-row effects*. International Journal of Computational Fluid Dynamics, Vol. 27, No. 2, pp. 88–99 (DOI:10.1080/10618562.2012.752074).

Yao, J., Gorrell, S.E., Wadia, A.R. (2008). *High-Fidelity Numerical Analysis of Per-Rev-Type Inlet Distortion Transfer in Multistage Fans: Part II–Entire Component Simulation and Investigation.* ASME Paper GT2008-50813.

Zhang, W., Vahdati, M. (2017). *Influence of the Inlet Distortion on Fan Stall Margin at Different Rotational Speed*. GPPS Paper 2017-0207.